



1 **Spatial–Seasonal Isotopic Variations in a Surface–Groundwater System in an**  
2 **Extremely Arid Basin and the Associated Hydrogeological Indications**

3 Yu Zhang<sup>1</sup>, Hongbing Tan<sup>1,\*</sup>, Peixin Cong<sup>1</sup>, Dongping Shi<sup>1</sup>, Wenbo Rao<sup>1</sup>, Xiying Zhang<sup>2</sup>

4 <sup>1</sup>School of Earth Sciences and Engineering, Hohai University, Nanjing 210098, China

5 <sup>2</sup>Qinghai Institute of Salt Lakes, CAS, Xining 810008, China

6 \* **Corresponding author:** Hongbing Tan (tan815@sina.com)

7 **Abstract**

8 Climate warming accelerates the global water cycle. However, the relationships between  
9 climate warming and hydrological processes in the alpine arid regions remain unclear. Herein,  
10 high spatiotemporal resolution sampling of surface water and groundwater was performed at the  
11 Qaidam Basin, an extremely arid area in the northeastern Tibetan Plateau. Stable H-O isotopes and  
12 radioactive <sup>3</sup>H isotopes were combined with atmospheric simulations to examine climate change  
13 and hydrogeological characteristics. The surface water heavy isotopes enrich during the wet season  
14 and deplete during the dry season. The contribution of precipitation to river discharge was  
15 considerably higher in the eastern region of the basin (approximately 45%) than in the central and  
16 western regions (10%–15%). The H-O isotopic compositions showed a gradually negative spatial  
17 pattern from the west to the east in the Eastern Kunlun Mountains water system; a reverse pattern  
18 occurred in the Qilian Mountains water system. This distribution pattern was jointly regulated by  
19 the westerly water vapor transport intensity and local hydrothermal conditions. Increased  
20 precipitation and cryosphere shrinkage caused by climate warming mainly accelerated basin  
21 groundwater cycle. In the eastern and southwestern Qaidam Basin, precipitation and ice/snow  
22 meltwater infiltrate structural channels that favor water flow, such as fractures and fissures,  
23 facilitating rapid seasonal groundwater recharge and increased terrestrial water storage. However,  
24 under future increases in precipitation in the southwestern Qaidam Basin, compensating for water  
25 loss from long-term melting of ice and snow will be challenging, and the total water resources may  
26 show an initially increasing and then decreasing trend.

27 **Keywords:** Qaidam Basin; isotope hydrology; water cycle; spatiotemporal pattern; climate



## 28 1. Introduction

29 Amidst the impending climate change process, an in-depth study of the hydrological cycle  
30 processes is a prerequisite for implementing water resource management and trend forecasting.  
31 Over the past half-century, continuous climate warming and intensified human activities have led  
32 to global water cycle acceleration and water resource redistribution at different scales ([Huntington](#)  
33 [et al., 2006](#); [Durack et al., 2012](#); [Masson-Delmotte et al., 2021](#)). For example, rapid warming has  
34 driven the rapid expansion of lakes in the Tibetan Plateau and the shrinking of lakes in the  
35 Mongolian Plateau ([Zhang et al., 2017](#)), and it has also amplified the severe shortage of irrigation  
36 water in parts of South Asia and East Asia ([Haddeland et al., 2014](#)). Moreover, it is expected to  
37 also reduce groundwater storage in the western region of the United States ([Condon et al., 2020](#)).  
38 At present, the arid regions of northwestern China are undergoing a change in climate from warm-  
39 dry to warm-humid ([Zhang et al., 2021](#)). The resulting uncertainties in alpine arid basin water  
40 resources in this region present new challenges in understanding the hydrological cycle and present  
41 state of water resources. These key scientific issues can be resolved by investigating the  
42 spatiotemporal distribution and driving mechanisms of surface and groundwater resources in the  
43 basin under accelerating climate warming.

44 The Tibetan Plateau, also known as the “Third Pole”, has complex cryosphere-hydrology-  
45 geodynamic processes and is especially susceptible to global warming ([Zhang et al., 2017](#); [Yao et](#)  
46 [al., 2022](#)). The Qaidam Basin is situated in the northeastern Tibetan Plateau and presents the largest  
47 extent of warming in the entire Tibetan Plateau and a substantial steep rise in temperature globally  
48 ([Li et al., 2015](#); [Kuang and Jiao, 2016](#); [Yao et al., 2022](#)). Since 1961, the average temperature of  
49 the basin has been rising at an alarming rate of 0.53°C/10 a as a result of climate warming ([Wang](#)  
50 [et al., 2014](#)), resulting in an increase in precipitation and retreat of the cryosphere in the region  
51 ([Song et al., 2014](#); [Xiang et al., 2016](#); [Zou et al., 2022](#)). These changes have led to rapid spatial  
52 changes in water storage in the Qaidam Basin, increased runoff or rising groundwater table in most  
53 parts of the region ([Jiao et al., 2015](#); [Wei et al., 2021](#)), and hydrological changes, such as the  
54 expansion of lakes, in the central and northern regions of the basin ([Ke et al., 2022](#); [Zhang et al.,](#)  
55 [2022](#)). However, several questions remain to be resolved: How are hydrological changes in the  
56 basin driven by climate changes? What are the potential influences of these changes on the water  
57 resources of the basin? These issues require an in-depth investigation. Rivers and groundwater  
58 carry precipitation and meltwater from high-altitude areas to the lakes in low-lying areas;



59 information on climate-hydrology dynamics of the runoff process can provide key evidence for  
60 the entire water cycle process. Hence, the Qaidam Basin is an excellent site for investigating the  
61 response mechanism of the hydrological cycle in the Tibetan Plateau caused by global warming.

62 Water isotopes (H and O) represent important components of water molecules and are useful  
63 natural environmental tracers of the water cycle and climate reconstruction, and they can help  
64 elucidate the processes that control water cycle changes, thus providing scientific evidence for  
65 human adaptations and effects on future global changes (Craig, 1961; Dansgaard, 1964; Yao et al.,  
66 2013; Bowen et al., 2019; Kong et al., 2019). Stable water isotope records provide key information  
67 on water migration processes, and they can compensate for the paucity of hydrometeorological,  
68 geological, and borehole data in hydrological research. Stable H-O isotopes and radioactive  $^3\text{H}$   
69 isotopes have been widely applied to quantify surface or groundwater recharge sources,  
70 interactions, budgets, and ages (Befus et al., 2017; Moran et al., 2019; Bam et al., 2020; Shi et al.,  
71 2021; Ahmed et al., 2022). Previous researchers have also performed a substantial amount of work  
72 on the use of isotopes to trace the water cycle in the Qaidam Basin (Xu et al., 2017; Xiao et al.,  
73 2017, 2018; Zhao et al., 2018; Tan et al., 2021; Yang and Wang, 2020; Yang et al., 2021). These  
74 studies have enhanced our understanding of aquifer properties in local regions and their recharge  
75 mechanisms. However, under the constraints of the harsh climate environment and  
76 hydrogeological survey accessibility in the Qaidam Basin, the water cycle processes in the basin  
77 in previous reports are mainly understood based on the watershed or confined regional unit scale.  
78 The use of regional research to achieve a comprehensive elucidation of the basin-scale water cycle  
79 mechanism is a challenge. Furthermore, the surface water and groundwater seasonal recharge  
80 information of the whole basin has not been systematically explored. Continuous changes in the  
81 topographical and tectonic spatial patterns of the basin are caused by various hydrological, climatic,  
82 and hydrogeological conditions; moreover, the hydrological effects exerted by anthropogenic  
83 climate change and regional aquifer properties differ seasonally (Jasechko et al., 2014). Therefore,  
84 it is particularly essential to study the entire process of basin water cycle and seasonal changes.  
85 While carrying out a comprehensive assessment of differences in isotopes of various potential  
86 recharge sources, it is fundamental to use the same technical methods for the systematic sampling  
87 and isotopic characterization of the basin.

88 In this study, the eight major watersheds of the Qaidam Basin were selected as the study sites  
89 and constraints were placed on the hydrological cycle patterns and processes of the Qaidam Basin

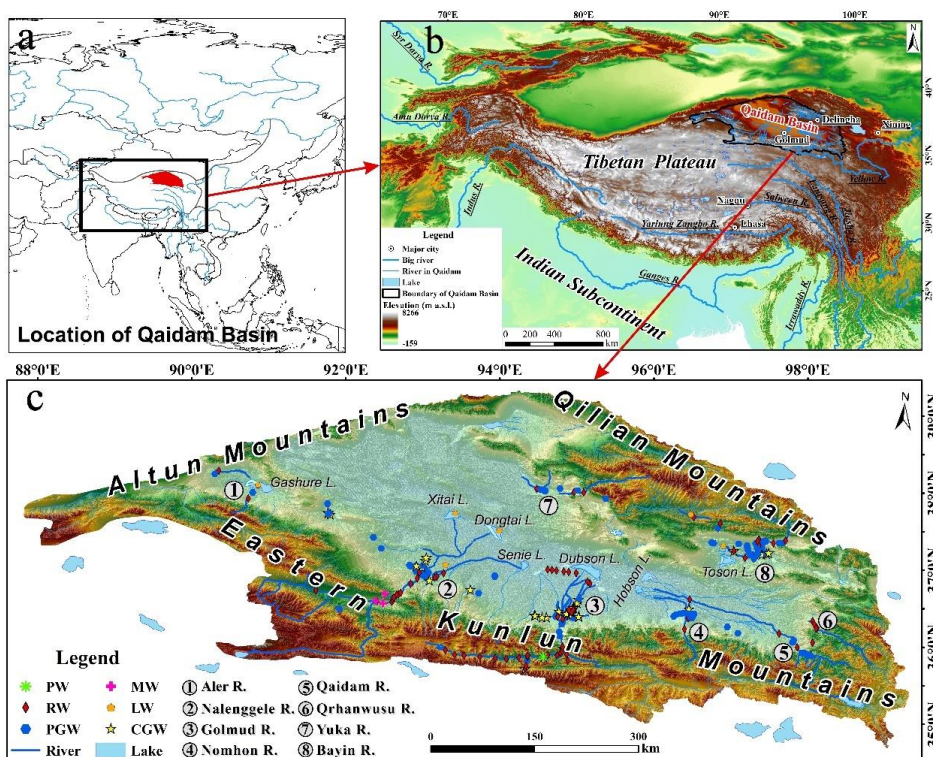


90 based on stable H-O isotope and radioactive  $^3\text{H}$  isotope data from the wet–dry season. The aims  
91 were to 1) elucidate the spatial–seasonal distribution pattern of surface–groundwater isotopes at  
92 different watershed scales in alpine arid basin; 2) analyze the composition changes of the Qaidam  
93 Basin water sources at different spatial–seasonal scales; 3) trace the entire water cycle process  
94 around the mountain–basin watersheds of the Qaidam Basin; and 4) predict the trend in the changes  
95 of Qaidam Basin water resources under the influence of a large extent of climate warming. The  
96 scientific contributions of this study include clarifying the isotope hydrology responses to climate  
97 change in the Tibetan Plateau arid basin, which is one of the ecosystems most affected by climate  
98 warming worldwide, from a microscopic scale; predicting the changing trend of water resources  
99 under the condition of multiple water sources recharge; and elucidating the entire water cycle  
100 process in extremely arid basins under the influence of rapid climate change.

## 101 2. Study area

### 102 2.1. General features

103 The Qaidam Basin is a closed and huge fault basin situated in the northeastern Tibetan Plateau  
104 (Figures 1a and 1b). With an area of approximately 250,000 km<sup>2</sup>, the basin is one of the four main  
105 basins in China, and it is surrounded by the Kunlun Mountains, Qilian Mountains and Altun  
106 Mountains. The Qaidam Basin has a plateau continental climate and represents a typical alpine  
107 arid inland basin that is characterized by drought. There are substantial variations in the basin  
108 temperature, and the average annual temperature is below 5 °C. The annual precipitation declines  
109 from 200 mm in the southeastern region to 15 mm in the northwestern region. The average annual  
110 relative humidity is 30%–40%, with a minimum lower than 5%. Modern glaciers have formed in  
111 the mountains on the southern and northern sides of the basin, which is surrounded more than 100  
112 rivers. Approximately 10 rivers are permanent, with most of the local rivers representing  
113 intermittent river systems. The rivers are mainly distributed on the eastern side of the basin but  
114 scant on the western side. The water in the basin lakes has become predominantly saline,  
115 comprising 31 salt lakes in total.



116

117 **Figure 1.** Location of Qaidam Basin (a, b) and the sampling sites (c)

118 2.2 Hydrogeology and structure

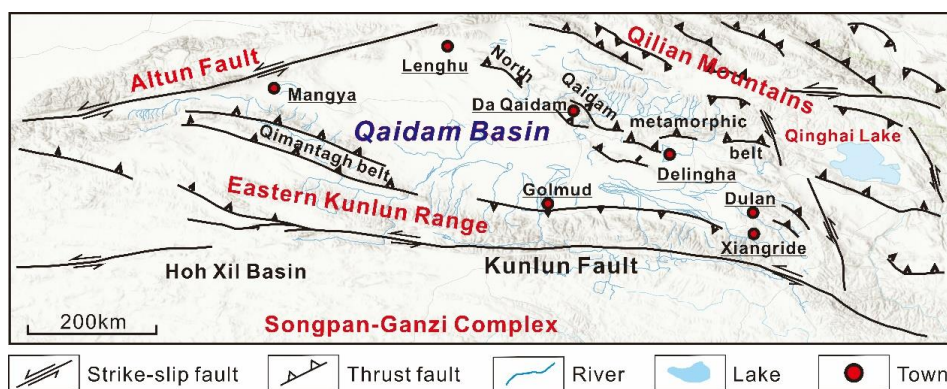
119 The basin basement consists of Precambrian crystalline metamorphic rock series, and the  
 120 caprock is of Paleogene-Neogene and Quaternary strata. The mountainous area surrounding the  
 121 basin is dominated by a Paleogene system, and the basin area and basin boundary zone are  
 122 characterized by a wide distribution of the Paleogene-Neogene system. The Quaternary system  
 123 is mainly distributed in the central basin region and the intermountain valley region. The basin terrain  
 124 is slightly tilted from the northwest to southeast, and the height gradually reduces from 3000 m to  
 125 approximately 2600 m. The distribution of the basin landforms presents a concentric ring shape.  
 126 From the edge to the center, the distribution of diluvial gravel fan-shaped land (Gobi), alluvial–  
 127 diluvial silt plain, lacustrine–alluvial silt clay plain, and lacustrine silt–salt plains follow a regular  
 128 pattern. Salt lakes are extensively distributed in low-lying terrains. The inner edge of the Gobi belt  
 129 in the northwestern basin region is clustered with hills that are less than 100 m in height. The



130 southeastern region of the basin has marked subsidence, and the alluvial and lacustrine plains are  
131 expansive. In the northeastern basin region, a secondary small intermountain basin has been  
132 formed between the basin and the Qilian Mountains by the uplifting of a series of low mountain  
133 fault blocks of metamorphic rock series.

134 The Qaidam Basin is situated in the Qin-Qi-Kun tectonic system, where there is strong  
135 neotectonic movement, and a series of syncline-anticline tectonic belts and regional deep faults  
136 have formed around it. The fault structures in the Qaidam Basin are very well developed and  
137 include the north-easterly Alun fault in the north; north-westerly Saishenteng–Aimunik northern  
138 margin deep fault in the northeast; westerly Qaidam northern margin deep fault in the northwest;  
139 Qimantag Mountains and Burhan Budai Mountains–Aimunik northern margin deep fault in the  
140 south; and north-westerly Sanhu major fault and north-easterly Qigaisu–Dongku Fault in the  
141 central basin region.

142 The basin water system distribution is subject to the constraints of the topography and  
143 neotectonic movements, and it appears to present an overall centripetal radial pattern ([Figure 1c](#)).  
144 There is frequent surface water–groundwater exchange, which is generally manifested as an  
145 abundance of precipitation and ice/snow meltwater in the mountainous areas, which are the main  
146 runoff areas. The runoff from the mountain flows through the Gobi belt in front of the mountain,  
147 with most of it infiltrating into the groundwater, subsequently flows over the surface in the form  
148 of confined artesian water or a spring at the front edge of the alluvial fan, and finally flows into  
149 the terminal lake. Groundwater can be roughly divided into bedrock fissure water, leached pore  
150 water and local confined groundwater, phreatic groundwater and confined artesian water, as well  
151 as salty phreatic groundwater, brine, and salty confined artesian water. Surface water and  
152 groundwater salinity and solutes are gradually enriched along this process ([Wang et al., 2008](#)).



153

154 **Figure 2.** Map of the Qaidam Basin tectonic distribution (modified after [Jian et al., 2020](#))

### 155 3. Sampling and methods

#### 156 3.1 Sampling and analysis

157 To elucidate the water cycle mechanisms in the Qaidam Basin, field investigations and  
158 sampling were carried out on the 8 major river–groundwater systems in the region from 2019 to  
159 2021. The sampling frequency of 6 watersheds essentially extends over a hydrological year and is  
160 represented by the wet season (July–August) and the dry season (March–April). Precipitation and  
161 snow meltwater were collected from the Eastern Kunlun Mountains. In total, 239 sampling points  
162 were established: phreatic groundwater (n = 100), confined groundwater (n = 43), spring water (n  
163 = 6), river water (n = 81), lake water (n = 5), snow meltwater (n = 3), and precipitation (n= 1). A  
164 total of 422 sets of samples were collected. No sampling point was established in the northwestern  
165 basin because the southern slope and front edge of the Altun Mountains consisted of tertiary system  
166 halite sedimentation and Quaternary system large salt flats, and no freshwater body is present.  
167 Therefore, the sample collection covers the entire Qaidam Basin and each of the major endorheic  
168 regions.

169 Hydrogen and oxygen isotope ( $^2\text{H}$ ,  $^3\text{H}$ , and  $^{18}\text{O}$ ) tests were conducted at the State Key  
170 Laboratory of Hydrology-Water Resources and Hydraulic Engineering, Hohai University, China.  
171 A MAT253 mass spectrometer was used to measure the ratios of  $^2\text{H}/^1\text{H}$  and  $^{18}\text{O}/^{16}\text{O}$ , and the results  
172 were compared with the Vienna Standard Mean Ocean Water (VSMOW), expressed in  $\delta$  (‰),  
173 with the analytical precision ( $1\sigma$ ) of the instrument for these isotopes was lower than  $\pm 1\text{‰}$  and  
174  $\pm 0.1\text{‰}$ . To determine the tritium ( $^3\text{H}$ ) concentration, the water sample was first concentrated by



175 electrolysis. Following sample enrichment, measurements were carried out using low background  
176 liquid scintillation counting (TRI-CARB 3170 TR/SL). The findings were expressed in terms of  
177 absolute concentration in tritium units (TU), the detection limit of the instrument was 0.2 TU, and  
178 the precision was improved to more than  $\pm 0.8$  TU.

### 179 3.2 Hydrograph separation

180 In the analysis of water sources among hydrological processes, endmember mixing models  
181 are widely used. According to the heterogeneity of different end member isotopes/water chemistry  
182 parameters, combined with the Bayesian mixing model, the contribution of each recharge end  
183 member to the mixed water body can be estimated (Hooper et al., 1990, 2003; Chang et al., 2018).  
184 The process is as follows:

$$185 \quad 1 = \sum_{i=1}^n f_i, \quad C_m^j = \sum_{i=1}^n f_i C_i^j, \quad j = 1, \dots, n \quad (1)$$

186 where  $f_i$  represents the proportion of water source  $i$ ,  $n$  represents the number of end members, and  
187  $C_m^j$  represents the level of tracer  $j$  in end member  $i$ .

188 Stable isotope analysis in R based on Bayesian mixing models (MixSIAR) can quantify the  
189 contributions of more than two potential endmembers (Parnell et al., 2010). In this study, based on  
190 the differences in the water body properties and isotopic composition of each endmember,  $\delta^{18}\text{O}$ ,  
191  $\delta\text{D}$ , and d-excess (d-excess =  $\delta\text{D} - 8\delta^{18}\text{O}$ ) data were used as parameters in the modeling. The  
192 model calculation process was carried out at a fractional increment of 1% and an uncertainty level  
193 of 0.1%.

### 194 3.3 Water vapor trajectory

195 The source and transport route of moisture can be monitored based on the water vapor flux  
196 field derived from the monthly mean ERA5 reanalysis data ( $0.25^\circ \times 0.25^\circ$ ) of the European Centre  
197 for Medium-Range Weather Forecasts (ECMWF, <https://www.ecmwf.int/>) (Hersbach et al., 2019).  
198 In this study, after taking into account that more than 70% of the precipitation in the Qaidam Basin  
199 occurs from June to September, the monthly mean ERA5 reanalysis data in this period from 2019  
200 to 2021 were used to analyze the water vapor transport path in and around the study area. Based  
201 on the average altitude of  $>3000$  m at the study site, the simulated atmospheric pressure was set to



202 500 hPa. The majority of the atmospheric water vapor was distributed in the range of 0–2 km  
203 above ground, and the simulated height did not have any remarkable influence on the findings (Li  
204 and Garzione, 2017; Yang and Wang, 2020).

## 205 4. Results

### 206 4.1 Stable H and O isotopes of different water bodies

207 The spatiotemporal changes of isotopes in the various water bodies in the entire basin are  
208 large, the watersheds have distinct characteristics, and considerable differences exist between  
209 surface water and groundwater. The  $\delta^{18}\text{O}$  and  $\delta\text{D}$  values extracted from the water samples of each  
210 watershed in the study region can be classified into six categories (Figure 3): 1) precipitation; 2)  
211 snow meltwater; 3) river water; 4) lake water; 5) phreatic groundwater; and 6) confined  
212 groundwater.

213 In the Qaidam Basin, the sources of precipitation are mainly concentrated on the northern and  
214 southern slopes of the Kunlun Mountains and Qilian Mountains, respectively. The ranges of  $\delta^{18}\text{O}$   
215 and  $\delta\text{D}$  of the precipitation samples from the Kunlun Mountains and Qilian Mountains (Zhu et al.,  
216 2015) were  $-23.38\text{‰}$  to  $+2.55\text{‰}$  and  $-158.64\text{‰}$  to  $+30.49\text{‰}$ , respectively. The corresponding  
217 fitted Local meteoric water line (LMWL) equation in the Qaidam Basin was  $\delta\text{D} = 7.48\delta^{18}\text{O} +$   
218  $11.30$  ( $R^2 = 0.95$ ,  $n = 74$ ), where the slope and intercept were similar to the long-term monitoring  
219 findings of the Qilian Mountains (Zhao et al., 2011; Gui et al., 2020; Wu et al., 2022; Yang et al.,  
220 2023). In the Qaidam Basin, the heavy isotopes present in snow meltwater samples were  
221 considerably depleted compared to rainwater. The  $\delta^{18}\text{O}$  and  $\delta\text{D}$  ranges were  $-19.30\text{‰}$  to  $-8.27\text{‰}$   
222 and  $-152.02\text{‰}$  to  $-53.52\text{‰}$  respectively, and the fitting trend equation was  $\delta\text{D} = 7.78\delta^{18}\text{O} + 10.85$   
223 ( $R^2 = 0.83$ ,  $n = 11$ ), with the slope and intercept lying between LMWL and GMWL (Global  
224 meteoric water line).

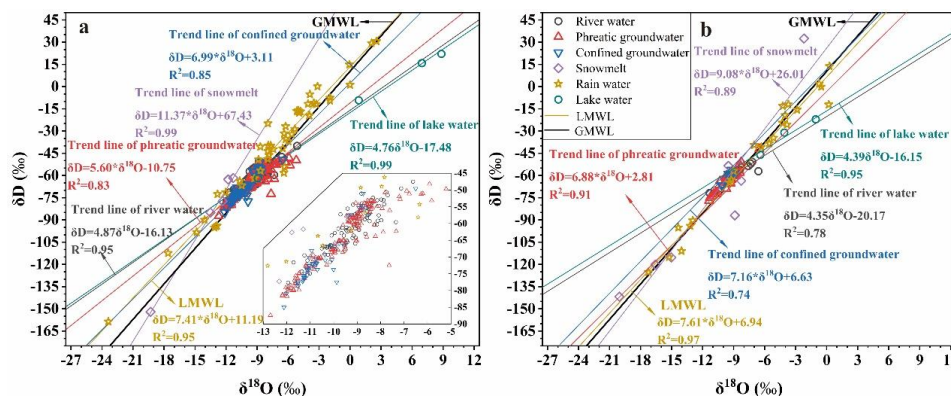
225 Among the surface water samples, the  $\delta^{18}\text{O}$  and  $\delta\text{D}$  ranges in river water were  $-13.51\text{‰}$  to  
226  $-5.93\text{‰}$  and  $-85.00\text{‰}$  to  $-47.50\text{‰}$  respectively, whereas those in the lake water were more  
227 enriched at  $-4.10\text{‰}$  to  $8.84\text{‰}$  and  $-31.05\text{‰}$  to  $22.07\text{‰}$ , respectively. The fitted trend lines of river  
228 and lake samples were:  $\delta\text{D} = 5.97\delta^{18}\text{O} - 5.54$  ( $R^2 = 0.85$ ,  $n = 92$ ) and  $\delta\text{D} = 4.64\delta^{18}\text{O} - 16.37$  ( $R^2$   
229  $= 0.99$ ,  $n = 7$ ), respectively, which were below both the GMWL and LMWL, indicating that the



230 surface water body has undergone varying extents of evaporation, with evaporation from lakes  
 231 being more enhanced.

232 In the groundwater samples, the H-O isotopic composition range was wider and considerable  
 233 differences occurred between phreatic and confined groundwater. The  $\delta^{18}\text{O}$  and  $\delta\text{D}$  value  
 234 distribution ranges in phreatic groundwater were  $-12.70\text{‰}$  to  $-5.21\text{‰}$  and  $-87.38\text{‰}$  to  $-42.00\text{‰}$ ,  
 235 respectively, and the fitted trend line was  $\delta\text{D} = 5.73\delta^{18}\text{O} - 9.20$  ( $R^2 = 0.83$ ,  $n = 185$ ). The phreatic  
 236 groundwater isotopic composition and slope of the trend line were similar to those of surface water,  
 237 indicating frequent interactions between the two and substantial evaporative fractionation of some  
 238 shallow groundwater. The  $\delta^{18}\text{O}$  and  $\delta\text{D}$  ranges in confined groundwater were relatively small and  
 239 lower in comparison at  $-12.12\text{‰}$  to  $-8.58\text{‰}$  and  $-85.00\text{‰}$  to  $-51.01\text{‰}$ . The linear regression  
 240 relationship of the samples fitting ( $\delta\text{D} = 7.84\delta^{18}\text{O} + 12.39$ ,  $R^2 = 0.87$ ,  $n = 51$ ) revealed that its  
 241 slope and intercept were essentially consistent with those of GMWL and LMWL, which suggests  
 242 the presence of a strong correlation between confined groundwater and atmospheric precipitation  
 243 in different periods.

244 Overall, in the Qaidam Basin, the stable H-O isotopic compositions of surface water and  
 245 groundwater were generally positively skewed. The isotopic composition and trend fitting  
 246 characteristics both demonstrated that the water samples have undergone varying extents of  
 247 evaporation during runoff, which reflects the cold and dry climate environmental characteristics  
 248 of the study area.

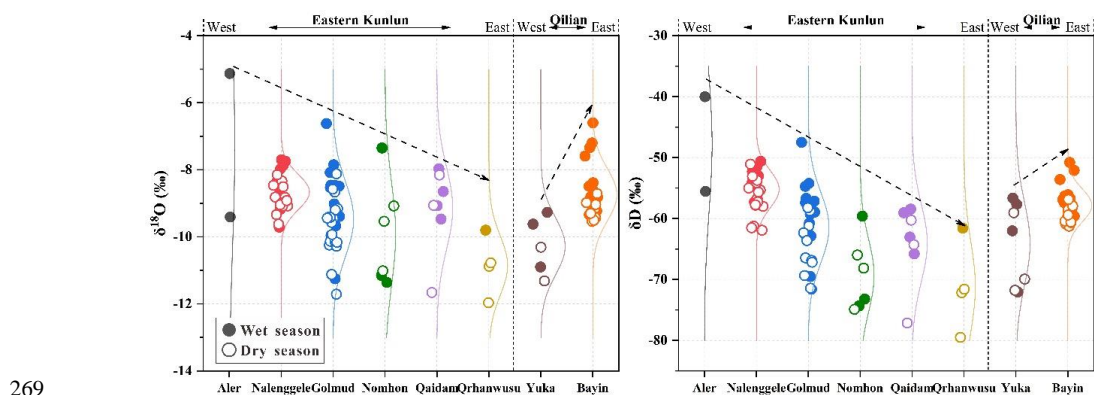


249  
 250 **Figure 3.** Diagram showing the relationship between  $\delta^{18}\text{O}$  and  $\delta\text{D}$  in different water bodies in the Qaidam Basin  
 251 (a. Eastern Kunlun Mountains water system; b. Qilian Mountains water system; The data of Rain water and  
 252 Snowmelt in the Qilian Mountains were from Zhu et al., 2015 and Yang et al., 2021, respectively)



#### 253 4.2 Spatial-seasonal characteristics of surface water $\delta^{18}\text{O}$ - $\delta\text{D}$

254 In the Qaidam Basin, considerable seasonal and spatial variations exist in the stable H-O  
255 isotopes of surface water (Figure 4). In terms of seasonal variation, apart from the Nomhon River,  
256 all watersheds displayed the characteristics of heavy isotope enrichment to varying extents during  
257 the wet season and relative depletion during the dry season. The basin surface water mean  $\delta^{18}\text{O}$   
258 and  $\delta\text{D}$  values were positively skewed by  $-0.08\text{‰}$  to  $1.08\text{‰}$  and  $0.63\text{‰}$  to  $10.58\text{‰}$ , respectively,  
259 in the wet seasons. Moreover, the seasonal variations of  $\delta^{18}\text{O}$  and  $\delta\text{D}$  were more pronounced in  
260 the downstream river compared to the upstream segment. For example, the  $\delta^{18}\text{O}$  value of the  
261 downstream Nomhon River was  $3.66\text{‰}$  higher during the wet season compared to the dry season.  
262 These phenomena reflect the differences in the recharge sources of the river during the wet–dry  
263 seasons and the strong surface evaporation effect in the central basin region. For spatial patterns,  
264 the isotopic composition of rivers originating from the Eastern Kunlun Mountains and Qilian  
265 Mountains had a contrasting distribution pattern, where the heavy isotopes of the Eastern Kunlun  
266 Mountains are gradually depleted in the direction of west to east, and the reverse held true for the  
267 Qilian Mountains. Of these, the  $\delta^{18}\text{O}$  and  $\delta\text{D}$  values were significantly positively skewed in the  
268 southwestern region of the basin and significantly negatively skewed in the eastern region.



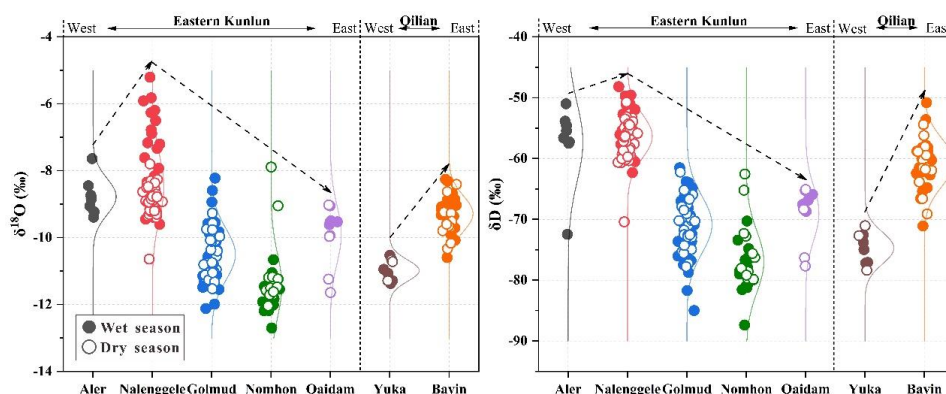
269  
270 **Figure 4.** Spatiotemporal variations in the H-O isotope composition of Qaidam Basin river water

#### 271 4.3 Spatial-seasonal characteristics of groundwater $\delta^{18}\text{O}$ - $\delta\text{D}$

272 The spatial variability of groundwater stable H-O isotopes was more pronounced compared  
273 with river water, although it did appear to follow the same distribution pattern as river water in the  
274 watershed (Figure 5). In terms of seasons, the  $\delta^{18}\text{O}$  and  $\delta\text{D}$  values in the groundwater system were



275 lower and seasonal fluctuations were smaller compared to that of the surface water. Specifically,  
276 the average seasonal variation of  $\delta^{18}\text{O}$  in each of the groundwater systems was in the range of  
277  $-0.75\text{‰}$  to  $+0.84\text{‰}$ , and the maximum seasonal variations in individual borehole were  $+3.31\text{‰}$   
278 and  $-3.16\text{‰}$ , respectively. This indicates that the groundwater isotopic composition was not  
279 entirely impacted by surface water infiltration. The region with the largest seasonal fluctuations of  
280 groundwater was located in the Nalenggele River in the southwestern basin, and the groundwater  
281 stable H-O isotopes in wet season were significantly more positively skewed compared to those  
282 of the dry season. Meanwhile, the region with the smallest seasonal variations of  $\delta^{18}\text{O}$  and  $\delta\text{D}$  is  
283 the adjacent Golmud River. Although there were no apparent differences in the topography and  
284 landforms of the two adjacent watersheds, significant differences were observed in the isotopic  
285 characteristics of the two. These phenomena reflect the following: 1) the kinetic fractionation of  
286 groundwater isotopes caused by evaporation and mixing was smaller than that of surface water  
287 isotopes; and 2) substantial differences were detected between the groundwater recharge and  
288 surface water–groundwater hydraulic interactions in each watershed.



289

290 **Figure 5.** Spatiotemporal variations in H-O isotopes in the groundwater of the Qaidam Basin

## 291 **5. Discussion**

### 292 **5.1 Water cycle information indicated by surface water isotopes**

293 Owing to the scant precipitation in the alpine arid region and its concentration in summer  
294 (June to September), the isotopic characteristics of surface water may reflect precipitation  
295 characteristics in the respective region during the wet season. The seasonal characteristics of stable  
296 H-O isotopes in the surface water, which consisted of enrichment during the wet season and



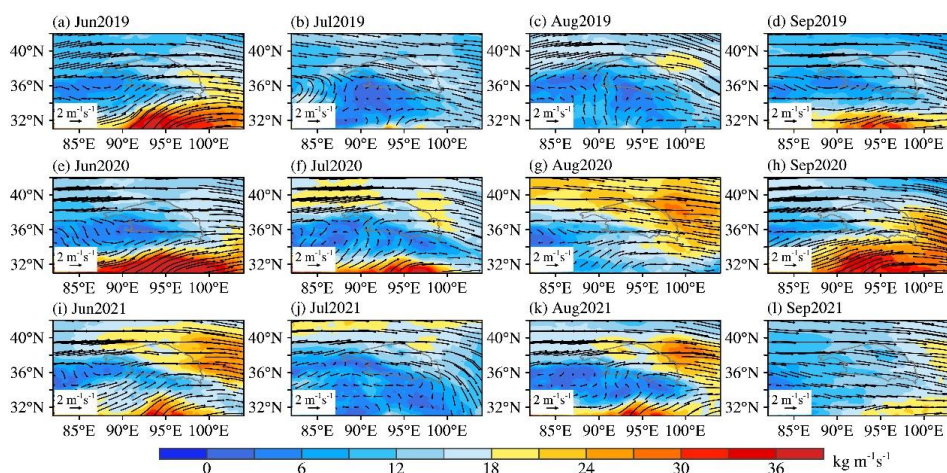
297 depletion during the dry season (Figure 4), were consistent with the observed–simulated patterns  
298 of changes in precipitation isotopes in the basin and its surrounding areas within each year (Liu et  
299 al., 2009; Zhao et al., 2011; Gui et al., 2020; Wu et al., 2022). In particular, the  $\delta^{18}\text{O}$  values at the  
300 sampling sites in the mountainous areas on the upper stream of each watershed were positive  
301 during the wet season compared to the dry season, which reflects the contribution of precipitation  
302 that is enriched in heavy isotopes to the river. Moreover, the mean  $\delta^{18}\text{O}$  and  $\delta\text{D}$  values were higher  
303 in watersheds (such as Qaidam and Bayin Rivers) during wet season, with corresponding greater  
304 precipitation (Figure S1). From this, it can be inferred that the river water stable H-O isotopes of  
305 each watershed in the basin were predominantly influenced by summer precipitation during the  
306 wet season. This is largely due to the wet season coinciding with the rainy season, where the  
307 relatively more concentrated rainfall may directly form surface runoff and rapidly recharge the  
308 river.

309 In the Eastern Kunlun Mountains water system, the spatial trend of river water H-O isotopes  
310 depletion from west to east (Figure 4) elucidates the variation of precipitation isotopes in relation  
311 to the water vapor transport process, which can be attributed to the waning of westerly winds.  
312 Along the water vapor transport path, heavy isotopes are preferentially separated in precipitation  
313 formation, leading to an augmentation in the continental characteristics of water vapor carried by  
314 the air mass, while the precipitation formed by the remaining water vapor undergoes a gradual  
315 depletion of isotopes (Yang and Wang, 2020). Meanwhile, the two watersheds in the Qilian  
316 Mountains possess contrasting spatial variation characteristics relative to the Eastern Kunlun  
317 Mountains water system. Based on the comparison and analysis of the meteorological elements of  
318 Delingha and Da Qaidam (refer to Figure 2 for specific location) from 2010 to 2020, the average  
319 annual precipitation of Delingha (276.36 mm) was 2.41 times higher than that of Da Qaidam  
320 (114.79 mm), and the average annual temperature of Delingha (5.23 °C) was higher than that of  
321 Da Qaidam (3.65 °C) by 1.58°C. Since 1961, precipitation in the Bayin River has risen by as much  
322 as 25.09 mm/10 a, which was more than six times greater than that of the Yuka River. Owing to  
323 the abundance and marked magnitude of increase of precipitation, the seasonal  $\delta^{18}\text{O}$  variation in  
324 the Bayin River was approximately 1.79 times that of the Yuka River. Under similar conditions  
325 where ice/snow meltwater recharge was present, the mean  $\delta^{18}\text{O}$  and  $\delta\text{D}$  values of the Bayin River  
326 were positively skewed by 1.52‰ and 7.26‰ relative to that of the Yuka River, respectively,  
327 which can be attributed to the greater contribution of precipitation with heavy isotopic enrichment



328 characteristics to the river water. Therefore, the spatial and seasonal variations of the river water  
329 H-O isotopes in the Qilian Mountains water system can be attributed to the variations in  
330 hydrothermal conditions and the varying extents of warming and humidification in the watershed.

331 To further explain the cause of seasonal and spatial variations of surface water  $\delta^{18}\text{O}$  and  $\delta\text{D}$   
332 values, ERA5 reanalysis data in the rainy season (June to September) were used to calculate the  
333 water vapor flux field in the Qaidam Basin and its surrounding areas and track the main paths of  
334 the water vapor transport of precipitation (Hersbach et al., 2019). The results (Figure 6)  
335 demonstrated that the water vapor path in and surrounding the basin is predominantly affected by  
336 the mid-latitude westerly air masses (Yang and Wang, 2020) and the water vapor flux in the eastern  
337 region of the basin is notably greater than that in the western region. This explains the spatial  
338 change patterns of river water H-O isotopes (Figure 4) and hydrothermal conditions to a large  
339 degree (Figure S1). The above findings are also supported by atmospheric and isotopic tracing  
340 evidences. For example, the Tanggula Mountains (33°–35° N) form the physical and chemical  
341 boundary of the Tibetan Plateau, and the northern region is fundamentally under the control of the  
342 westerly wind, which hinders the South Asian monsoon from exerting a direct influence on the  
343 Qaidam Basin (Yao et al., 2013; Kang et al. 2019; Wang et al., 2019). Furthermore, water vapor  
344 source information can be reflected in d-excess, where the recycled moisture that evaporated under  
345 conditions of low humidity and water carried by the westerly wind is considered to possess higher  
346 d-excess values. The mean d-excess of basin river water samples during the wet season (11.45‰,  
347 Table S1) was greater than 10‰, which reflects the characteristics of an alpine arid continental  
348 climate and a water vapor source devoid of monsoon influences. In contrast, in the hinterland of  
349 the Tibetan Plateau, south of the Tanggula Mountains, which is subject to considerable influences  
350 from the South Asian monsoon circulation, the d-excess values of summer precipitation and river  
351 water were in the range of 5‰–9‰, with mean value of 7‰ (Tian et al., 2001). The substantial  
352 differences in the d-excess values between the two regions also support the above inference about  
353 the water vapor sources of the Qaidam Basin.



354

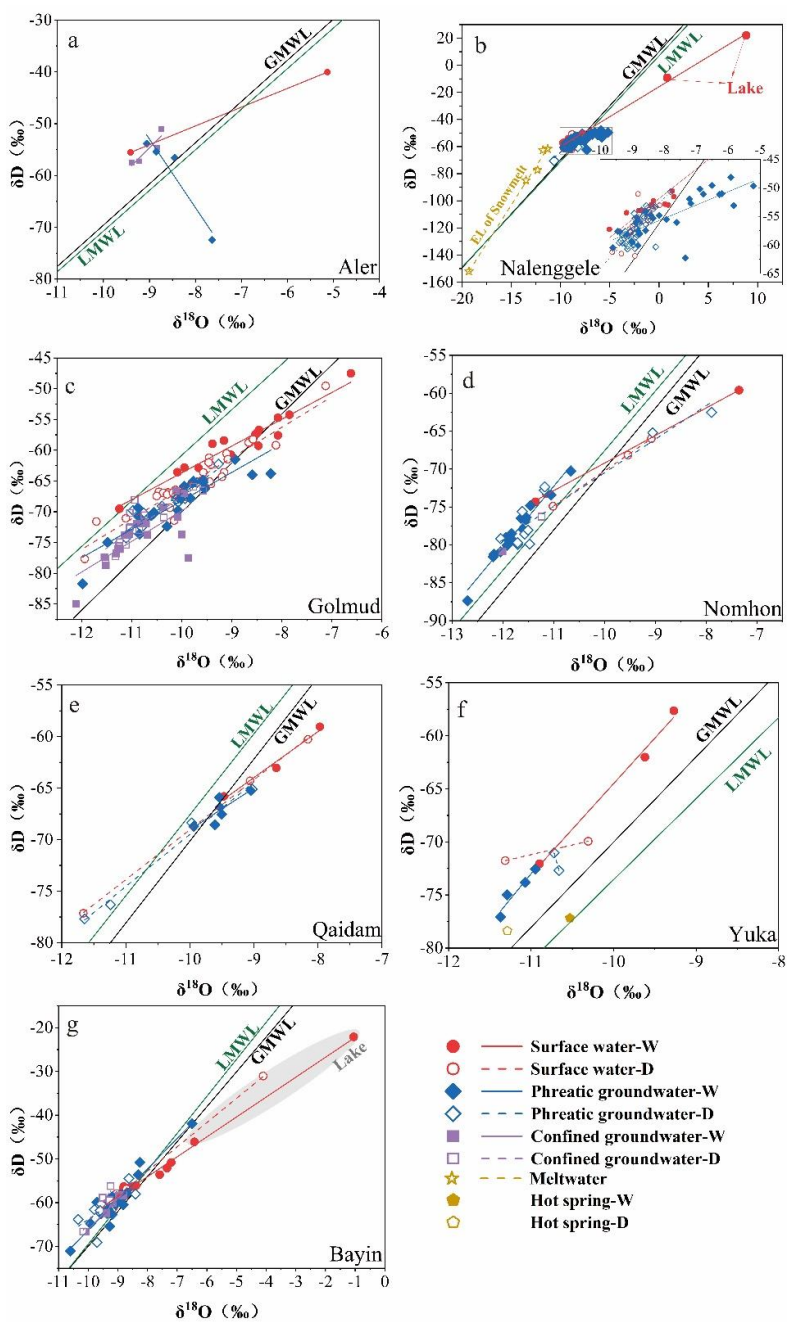
355 **Figure 6.** Tropospheric water vapor flux from June to September 2019 to 2021 (below 500 hPa, unit:  $\text{kg m}^{-1} \text{s}^{-1}$ )

356 Given the spatiotemporal differences of surface water  $\delta^{18}\text{O}$ - $\delta\text{D}$  (Figure 4), samples of  
357 different water bodies in each watershed were incorporated into the  $\delta^{18}\text{O}$ - $\delta\text{D}$  plot (Figure 7). The  
358 presence of considerable differences in isotope distribution characteristics suggests that seasonal  
359 changes in the surface water H-O isotopes in each water type may be due to differences in the  
360 proportions of the contribution of precipitation, ice/snow meltwater, and groundwater during the  
361 wet and dry seasons. Hence, Equation 1 (Table 1) was employed to estimate the contribution of  
362 each potential recharge endmember to the river water. The findings indicated that in the dry season,  
363 the base flow in each watershed is maintained by the groundwater discharge in mountainous areas,  
364 where the contribution of groundwater to base flow may reach up to 97%. During the wet season,  
365 the river water in each watershed is recharged by different proportions of precipitation, ice/snow  
366 meltwater and groundwater. For example, in the area with the most abundant annual rainfall, the  
367 contribution of precipitation to the Bayin River may reach 84% during the wet season. The  
368 westerly water vapor forms more precipitation as a result of obstruction from landforms in the  
369 eastern region of the basin, in contrast, as the source area of the Bayin River is in close proximity  
370 to the eastern region of Qilian Mountains, although the summer monsoon is likened to ‘an arrow  
371 at the end of its flight’ (a spent force), the latter continues to contribute more than 22% of the  
372 oceanic water vapor to the nearby areas (Wu et al., 2022). The topographic obstruction and strong  
373 convection form abundant precipitation, rendering the proportion of precipitation in the surface  
374 runoff in the eastern basin region appreciably higher than that in other areas. Thus, differences in



375 the proportions of contribution ratio of each recharge end member during wet and dry seasons are  
376 the main factors responsible for the seasonal variations in surface water isotopes in each watershed.

377 In summary, the seasonal variations and spatial patterns of surface water stable H-O isotopes  
378 are a consequence of the combined effects of the extent of warmth and humidity in the region,  
379 intensity of the mid-latitude westerly wind water vapor transport, and local hydrometeorological  
380 conditions.



381

382 **Figure 7.**  $\delta^{18}O$ - $\delta D$  plots during dry-wet seasons and in different water bodies in each watershed of the Qaidam  
 383 Basin (W and D represent wet and dry seasons, respectively)



384 **Table 1.** Contribution ratios of endmembers to river water during the wet and dry seasons based on  $\delta^{18}\text{O}$  and  
 385  $\text{d}$ -excess (Unit: %; W and D represent wet season and dry season, respectively)

	Endmember	Groundwater	Meltwater	Tributary	Precipitation
Nalengele-W	Mean	0.41		0.47	0.12
	Max	0.60		0.74	0.13
	Min	0.18		0.27	0.08
	SD	0.12		0.13	0.02
Nalengele-D	Mean	0.90	0.10		
	Max	0.97	0.27		
	Min	0.73	0.03		
	SD	0.07	0.07		
Golmud-W	Mean	0.31	0.34	0.25	0.10
	Max	0.36	0.39	0.32	0.12
	Min	0.28	0.29	0.20	0.08
	SD	0.03	0.04	0.05	0.01
Golmud-D	Mean	0.32	0.25	0.42	
	Max	0.46	0.45	0.70	
	Min	0.19	0.11	0.21	
	SD	0.09	0.10	0.17	
Yuka-W	Mean	0.62	0.23		0.15
	Max	0.76	0.29		0.18
	Min	0.55	0.15		0.10
	SD	0.10	0.06		0.04
Bayin-W	Mean	0.26	0.04	0.25	0.45
	Max	0.35	0.05	0.43	0.84
	Min	0.08	0.02	0.06	0.23
	SD	0.08	0.01	0.11	0.19

386 5.2 Sources and spatial patterns of groundwater recharge

387 The seasonal variations in groundwater aquifer H-O isotopes in each watershed suggests that  
 388 differences exist in their recharge sources, forms, and rates. The  $\delta^{18}\text{O}$ - $\delta\text{D}$  relationship of different  
 389 seasons and different types of water samples can be used to elucidate the groundwater source  
 390 composition and recharge pattern. The Qaidam Basin groundwater system can be classified into  
 391 three types of recharges according to the seasonal changes in groundwater  $\delta^{18}\text{O}$ - $\delta\text{D}$  in each  
 392 watershed (Figure 5) as well as the  $\delta^{18}\text{O}$ - $\delta\text{D}$  relationship of different water bodies within the  
 393 watershed (Figure 7).



394 5.2.1 Heavy precipitation in the wet season-dominated recharge

395 In the Nalenggele River, which is situated in the southwestern basin, and the Qaidam and  
396 Bayin Rivers in the eastern basin, groundwater  $\delta^{18}\text{O}$  and  $\delta\text{D}$  values were markedly positively  
397 skewed during the wet season. The groundwater isotope data distribution in the majority of the  
398 wet seasons was closer to the LMWL and GMWL compared to that during the dry season.  
399 Moreover, the isotopic characteristics were closer to the river water and summer precipitation in  
400 the same period (Table S1; Zhu et al., 2015), with different trends in evaporation (Figures 7b, 7e  
401 and 7g). These results indicate the contribution of precipitation to groundwater during the wet  
402 seasons. The relatively marked seasonal variations of H-O isotopes also demonstrate that the  
403 aquifers in the eastern and southwestern Qaidam Basin have a relatively rapid groundwater cycle  
404 and present seasonal recharge. In the eastern basin, there is an abundance and notable rise in  
405 precipitation (Figure S1), which has directly led to a rise of 5 m in water level and surface area  
406 expansion of 1.59 times in a lake at the source of the Nalenggele River in the southwestern basin  
407 from 1995 to 2015 (Chen et al., 2019). This further indicates the abundant precipitation in the  
408 headwater may be a potential source for the rapid seasonal recharge of groundwater recharge  
409 associated with the rapid climate warming and humidification. Additionally, the tectonic  
410 conditions of the recharge area are factors that are in favor of driving seasonal groundwater  
411 recharge. These three watersheds happened to be situated in the collision zone (Figure 2), where  
412 neotectonic movement is strong, and there are substantial developments of deep fractures and  
413 faults in the recharge area. It can be inferred from the aforementioned that favorable hydrological  
414 and tectonic conditions promote the formation of direct and rapid recharge of groundwater through  
415 bedrock fissures under the large hydraulic head (>1000 m) from precipitation and meltwater at  
416 higher altitudes, resulting in substantial seasonal changes in the groundwater H-O isotopes in these  
417 regions (Tan et al., 2021).

418 5.2.2 Glacial-snow melt water-dominated recharge

419 In the Nomhon and Yuka Rivers situated in the central basin region, groundwater H-O  
420 isotopes were more depleted during the wet season compared to the dry season (Table S1; Figure  
421 5). Figures 7d and 7f also show that the majority of the  $\delta^{18}\text{O}$ - $\delta\text{D}$  data for the groundwater samples  
422 in these two watersheds were observed in the lower left of the LMWL and GMWL. These values  
423 were far away from the LMWL and GMWL, and were more negatively skewed relative to river



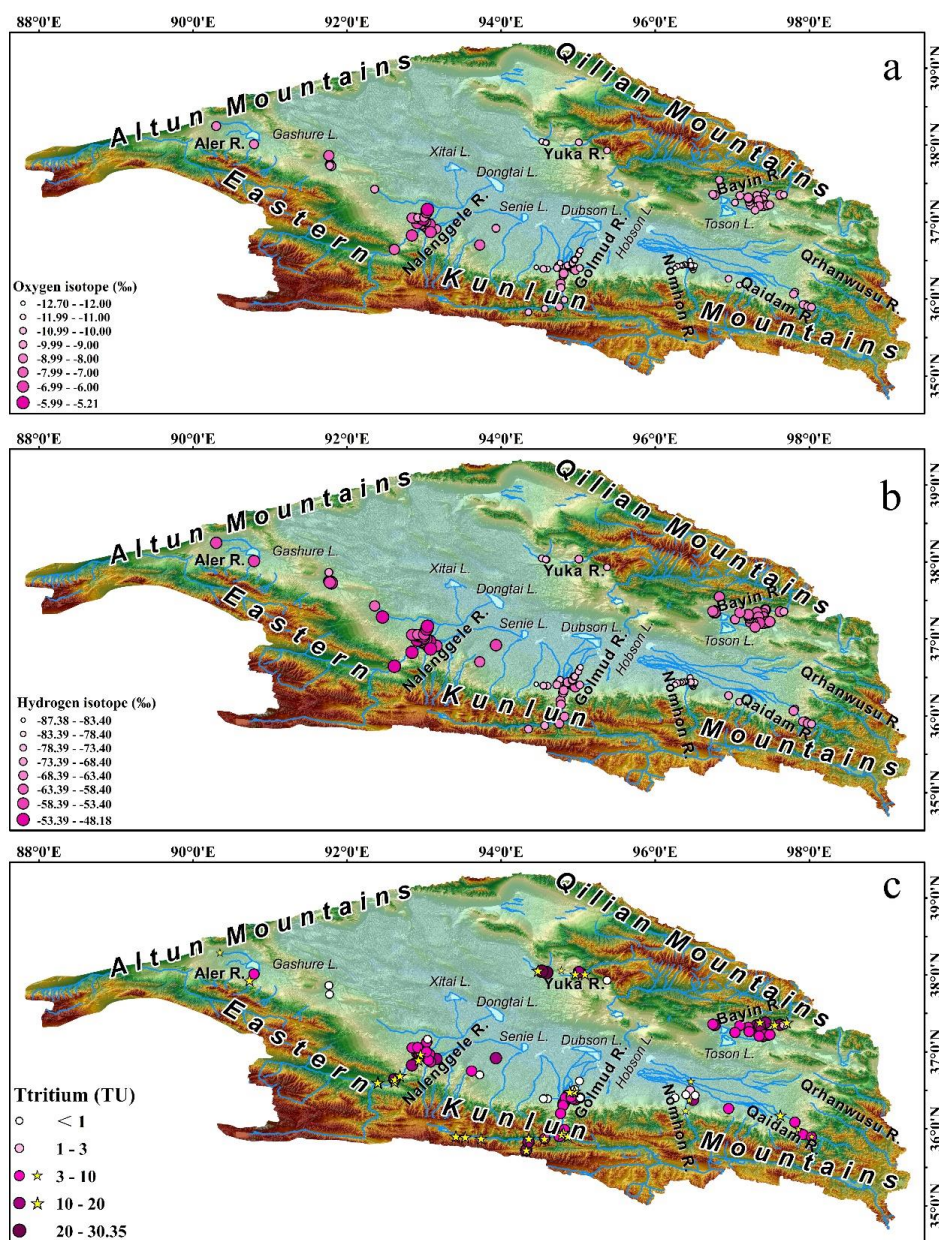
424 water, with characteristics being closer to the snow meltwater observed in the high-altitude Eastern  
425 Kunlun Mountain (Figure 3; Yang et al., 2016). This demonstrates that the groundwater recharged  
426 by ice/snow meltwater was more depleted in heavy isotopes during the wet–dry seasons and the  
427 contribution of precipitation to the aquifer was relatively small. Similarly, on the eastern margin  
428 of the Tibetan Plateau, the phenomenon where the non-monsoon meltwater controls the monsoon  
429 groundwater system hydrological process has been observed (Kong et al., 2019). The isotope  
430 signals indicated that ice/snow meltwater depleted in the heavy isotopes in the source area was  
431 released as a result of the rising temperature in summer, and following the mixing of groundwater  
432 with the seasonal meltwater recharge, the groundwater was further depleted in heavy isotopes.  
433 Furthermore, owing to the low precipitation in these two watersheds (61.39 and 121.78 mm, Figure  
434 S1), the precipitation in 2020 was even lower. Under extremely arid climate, the direct recharge  
435 to the aquifer from the limited precipitation was negligible. GRACE data also showed that the  
436 melting of solid water in the source area due to climate warming was a key factor driving the  
437 increase in the groundwater storage of the Qaidam Basin (Xiang et al., 2016). This further supports  
438 the inference that groundwater isotopic depletion during the wet season stems from the seasonal  
439 melting recharge of the cryosphere.

#### 440 5.2.3 Fossil water-dominated recharge

441 In the Golmud River, the mean  $\delta^{18}\text{O}$  value during the wet season was 0.33‰ higher than that  
442 during the dry season and seasonal changes were not apparent, indicating that the proportion of  
443 seasonal groundwater recharge was small and the renewal rate was slow. The H-O isotope data of  
444 the groundwater were mainly located between the LMWL and GMWL (Figure 7c), indicating that  
445 the main recharge source was the atmospheric precipitation of different seasons. In addition, the  
446 groundwater  $\delta^{18}\text{O}$  and  $\delta\text{D}$  in the alluvial fan belt exhibited a gradually negatively skewed trend  
447 along the flow path (Figures 8a and 8b). A prominent feature of this watershed is the sizeable  
448 storage of confined groundwater, which is continuously emanating at the front edge of the alluvial  
449 fan. Confined groundwater possesses  $\delta^{18}\text{O}$  and  $\delta\text{D}$  values that are more negative than phreatic  
450 groundwater, and the mean  $\delta^{18}\text{O}$  values during the wet–dry seasons are consistent, without any  
451 seasonal changes. The substantial differences in isotopic characteristics between phreatic and  
452 confined groundwaters (Table S1) suggest that there are potential differences in their recharge  
453 sources. It is speculated that phreatic groundwater is predominantly recharged by ice/snow



454 meltwater while confined groundwater is slowly and stably recharged and may be sustained by  
455 precipitation with low  $\delta^{18}\text{O}$  and  $\delta\text{D}$  values or fossil water formed under the relatively cold climatic  
456 conditions (Xiao et al., 2018).



457



458 **Figure 8.** Spatial distribution of groundwater  $\delta^{18}\text{O}$  (a) and  $\delta\text{D}$  (b), and surface water–groundwater  $^3\text{H}$  (c)  
459 concentrations during the wet season (Circle and asterisk represent groundwater and surface water, respectively)

### 460 5.3 Water cycle mechanism

461 Being a direct constituent of water molecules, radioactive  $^3\text{H}$  with a half-life of 12.32 years  
462 can be used to estimate the migration time of younger water. Particularly,  $^3\text{H}$  can effectively trace  
463 groundwater age and renewal rate in water bodies consisting of a mix of younger water and fossil  
464 water (Xiao et al., 2018; Chatterjee et al., 2019; Shi et al., 2021). In accordance with the  
465 considerable differences in  $\delta^{18}\text{O}$ - $\delta\text{D}$  of the different water bodies in each watershed (Figures 7, 8a  
466 and 8b), the scale and extent of the groundwater recharge in the Qaidam Basin were further  
467 determined using the  $^3\text{H}$  concentration. The  $^3\text{H}$  concentration spatial distribution pattern indicated  
468 that there were considerable differences in groundwater recharge rates at both intra- and inter-  
469 watershed scales (Figure 8c). Thus, the groundwater system was dominated by both regional and  
470 local recharge.

471 At the watershed scale, the  $^3\text{H}$  concentration of the phreatic groundwater in the alluvial fan  
472 zone near the river channel and mountain pass was considerably higher (Table S1) and close to  
473 that of the river water. These results indicate that close hydraulic interactions occurred between  
474 the surface water and groundwater and the aquifer also receives river water via vertical infiltration  
475 and lateral runoff recharge. Hence, this portion of groundwater is dominated by seasonal modern  
476 water recharge, which is younger and has a relatively more rapid renewal rate. The phreatic and  
477 confined groundwater  $^3\text{H}$  concentrations at the edge of the alluvial fan were largely below 3 TU  
478 or lower than the detection limit, which was inconsistent with that near the river channel. These  
479 findings suggest that these aquifers are predominantly recharged by lateral runoff, which consists  
480 largely of submodern water (>60 years) or fossil water, and the mixing proportion of modern  
481 precipitation and seasonal meltwater is relatively low, with a slow renewal rate. This situation is  
482 particularly apparent in Golmud and Nomhon Rivers (Liu et al., 2014; Cui et al., 2015; Xiao et al.,  
483 2017, 2018), which also further reflects the importance of fossil water content in maintaining the  
484 aquifer in extremely arid regions.

485 At the basin scale, radioactive  $^3\text{H}$  concentration characteristics are consistent with the water  
486 cycle information indicated by the seasonal changes in stable H-O isotopes. In the phreatic  
487 groundwater systems situated in the eastern and southwestern basin regions,  $^2\text{H}$  and  $^{18}\text{O}$  are

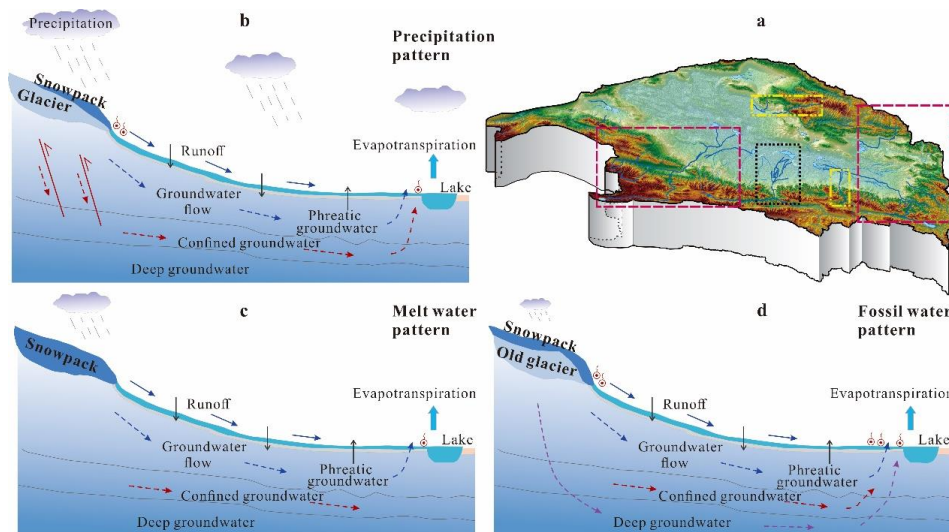


488 relatively enriched during the wet season,  $^3\text{H}$  has a relatively higher average concentration,  
489 seasonal groundwater recharge is more noticeable, and groundwater is overall younger (<60 years).  
490 Based on river seepage, modern meltwater and precipitation may also infiltrate through favorable  
491 structural water passage channels, such as fault zones developed on a large scale in the recharge  
492 area, resulting in rapid recharge to the aquifer (Figure 9b; Tan et al., 2021). The phreatic  
493 groundwater systems in the western Qilian Mountains and central Eastern Kunlun Mountains were  
494 relatively depleted in  $^2\text{H}$  and  $^{18}\text{O}$  during the wet season, the  $^3\text{H}$  concentrations were  
495 correspondingly low, and these systems mainly received recharge from seasonal ice/snow  
496 meltwater. However, due to the relatively stable recharge of meltwater by comparison, the  
497 groundwater renewal rate was relatively slow (Figure 9c).

498 The depletion of heavy H-O isotope was greatest in confined groundwater, and the  $^3\text{H}$   
499 concentration of the majority of the samples was very low (<3 TU) or fall below the detection limit,  
500 which indicates that the confined groundwater recharge rate is very slow. Furthermore, the  
501 confined groundwater was largely over 100 years old and consisted predominantly of submodern  
502 groundwater or fossil water (Xiao et al., 2018). In the Golmud River, the effect of H-O isotope  
503 seasonal changes in most of the confined groundwater was relatively small or showed almost no  
504 detectable change. However, the confined groundwater in the overflow zone continued to  
505 spontaneously emanate after nearly half a century of mining and the water pressure did not  
506 decrease, which suggests that modern precipitation or ice/snow meltwater recharges deep confined  
507 groundwater. Some confined groundwaters possess recognizable isotopic seasonal effects, and the  
508 existence of a certain proportion of continuous recharge, even on a seasonal scale, cannot be ruled  
509 out. In addition, large karst springs have developed in the mountainous areas of the Golmud River.  
510 Moreover, a large karst spring (KLSQ-1) was observed near the mountain pass, with a flow rate  
511 as high as 224.7 L/s. In mountainous areas, well-formed karst cavities and fissures provide  
512 conduits to enable the direct infiltration of precipitation or meltwater. Following deep circulation,  
513 precipitation and meltwater give rise to regional subsurface runoff, which recharges confined  
514 groundwater in the overflow zone over a long distance, thus causing it to flow continuously under  
515 the effect of a large hydraulic head (approximately 1,000 m) (Figure 9d). Moreover, in the Golmud  
516 and Bayin Rivers, the H-O isotopic signals of some confined groundwaters at the front edge of the  
517 alluvial fan were essentially consistent with that of the nearby phreatic groundwater and the  $^3\text{H}$



518 concentration was close to 10 TU. These findings also suggest that the confined groundwater may  
519 pass through the aquitard or leakage recharge occurs in the local skylights.



520

521 **Figure 9.** Schematic diagram of the Qaidam Basin water cycle model (b represents the blue dashed box; c  
522 represents the yellow dashed box; and d represents the black dashed box)

#### 523 5.4 Isotope hydrology responses and water cycle trends under climate change

524 Since the 1980s, the Qaidam Basin has experienced rapid warming at a rate more than twice  
525 the global average (Wang et al., 2014; Kuang and Jiao, 2016; Yao et al., 2022). Since 1960, average  
526 annual temperature and precipitation variations and increasing rates over every 10 and 30 years at  
527 eight meteorological stations in the basin (Figure 10a) and continuous air temperature and  
528 precipitation change trends at two representative meteorological stations in the north and south  
529 (Delingha and Golmud) (Figure 10b) have shown that the present warming and humidification  
530 trends in the northeastern Tibetan Plateau are continuously strengthening. Previously, the general  
531 assumptions were that the isotopic composition of the surface water and groundwater systems did  
532 not vary with time, at least on interannual scales, and was relatively stable (Boutt et al., 2019).  
533 However, over the past 40 years, the isotopic variations of water bodies have demonstrated that  
534 varying degrees of interannual differences in surface water and groundwater isotopes exist and  
535 interannual variations in the average  $\delta^{18}\text{O}$  value are greater than 3‰ (Figure 11). Therefore,  
536 isotopic changes reflect different extents of sensitivity to climate change, regardless of the seasonal  
537 or multi-year scale. The spatiotemporal variability of isotopic signals can be ascribed to differences

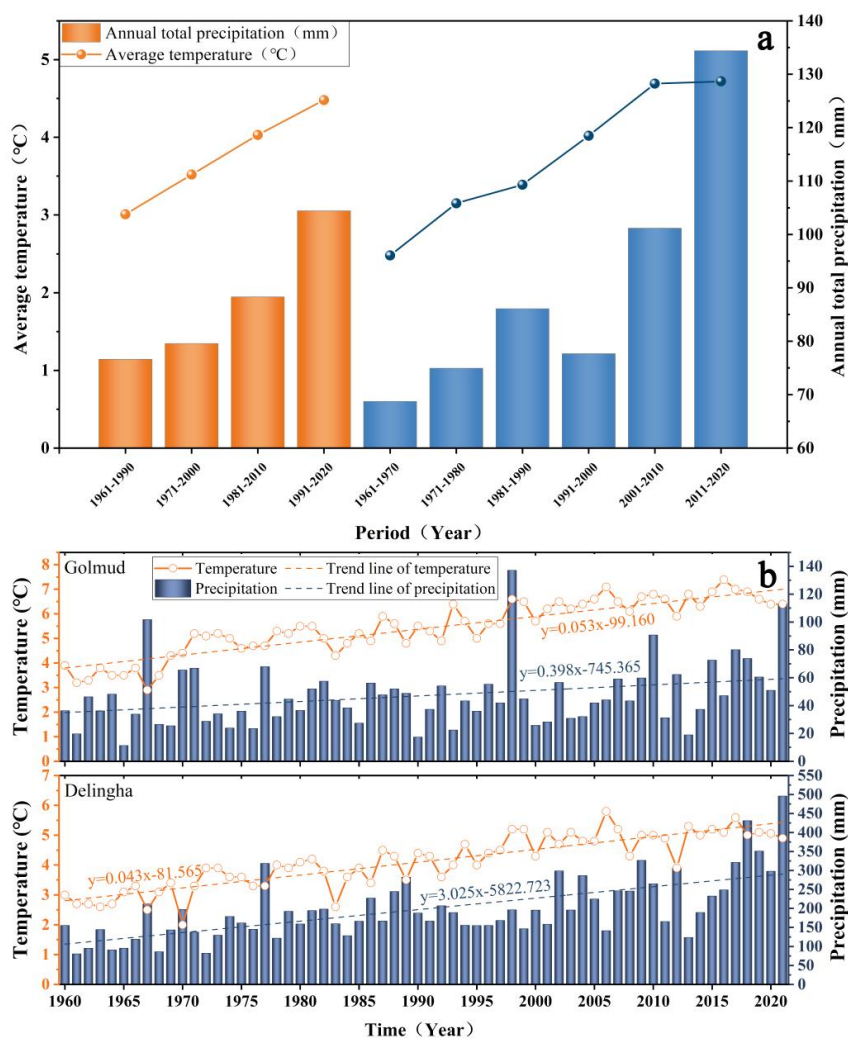


538 in the extent of warming and humidification in each watershed. Wang et al. (2014) highlighted  
539 that while the Qaidam Basin has experienced rapid warming in the past 50 years, the extent of  
540 warming and humidification in different regions is noticeably not in sync, where the rate of  
541 temperature rise ranged from 0.31 to 0.89°C/10a and the rate of rainfall increase ranged from 1.77  
542 to 25.09 mm/10a (Figure S1). The correlation between  $\delta^{18}\text{O}$  of watershed surface-groundwater  
543 and temperature and precipitation showed (Figure 12) that the multi-year scale  $\delta^{18}\text{O}$  variations in  
544 the basin surface water and groundwater had a more significant positive correlation with  
545 precipitation in the same period than temperature (Figures 12b and 12d). Of note, surface water  
546 was more sensitive to precipitation (Figures 12a and 12b) while groundwater was more sensitive  
547 to temperature (Figures 12a and 12c). This phenomenon suggests that the rise in rainfall may affect  
548 the water cycle by promoting slope runoff and groundwater infiltration in mountainous regions  
549 and indicates that warming will lead to the ablation of solid water at higher altitudes to accelerate  
550 the groundwater recharge of aquifers through bedrock fissures. The GRACE and remote sensing  
551 monitoring findings also demonstrated that the increase in terrestrial water storage in the Qaidam  
552 Basin is closely linked to the rise in rainfall and glacier meltwater recharge (Song et al., 2014; Jiao  
553 et al., 2015; Xiang et al., 2016; Wei et al., 2021; Zou et al., 2022), which fully supports the isotope-  
554 based conjecture. Furthermore, recent research demonstrates that the accelerated conversion of ice  
555 and snow on the Tibetan Plateau into liquid water has led to an imbalance in the “Asia Water  
556 Tower”, with the Qaidam Basin one of the major regions experiencing an increase in liquid water  
557 (Yao et al., 2022). The consistency of data on H-O isotopes, remote sensing and hydrometeorology  
558 shows that the Qaidam Basin is a region in the Tibetan Plateau with the most rapid and substantial  
559 warming. Global warming affects the basin by causing a redistribution of precipitation and melting  
560 ice and snow in high-altitude areas, resulting in a rise in groundwater storage and an expansion of  
561 the area of lakes, among other effects. Additionally, the corresponding rise in precipitation in the  
562 mountainous areas is able to supplement the rapidly melting ice and snow to a certain degree. This  
563 trend of water storage increase in the Qaidam Basin is likely to continue in the 21st century. The  
564 highly coupled findings of different observation methods further emphasize the sensitivity and  
565 potential of water stable isotopes in tracing water cycles and climate change.

566 Due to the effects of climate change and the intensification of cryosphere retreat, runoff has  
567 changed considerably on the Tibetan Plateau, which drastically impacted the spatiotemporal  
568 distribution of water resources (Wang et al., 2021). Based on our observation results, it can be

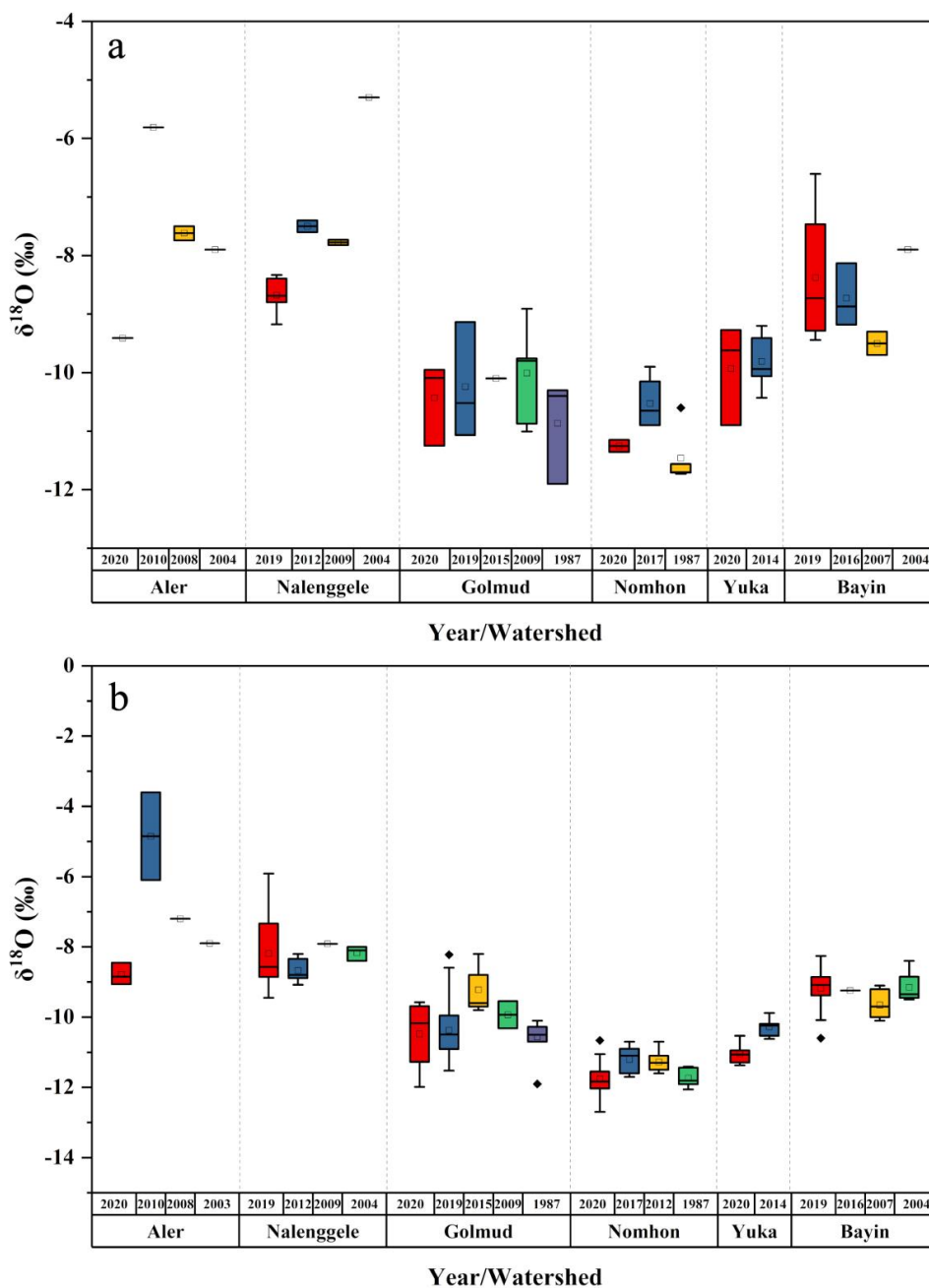


569 speculated that with continued rapid warming and humidification, the water resources of the  
570 watershed with substantial seasonal recharge may manifest as follows: The amount of surface  
571 water and groundwater resources will considerably increase in the short term (in recent decades)  
572 because of the shift of snow line and rapid melting of ice and snow coupled with the increase in  
573 precipitation. For example, in the Bayin and Qaidam Rivers in the eastern basin, as a result of the  
574 abundant and marked increase in precipitation and strong water resource renewal capability, the  
575 water reserves may sustain an increasing trend in the long term under the influence of continuous  
576 climate warming. This phenomenon has been verified in many regions of the Tibetan Plateau and  
577 some alpine watersheds in high-latitude Switzerland (Xiang et al., 2016; Malard et al., 2016; Shi  
578 et al., 2021). Moreover, the cyclical nature of climate change also suggests that cryosphere retreat  
579 on a large scale may not be sustainable for watershed surface–groundwater recharge. It was  
580 reported that the glaciers in the southwestern basin are continuously losing mass (−0.2 to −0.5  
581 m/a), and this trend has substantially increased from 2018 to 2020, particularly in the headwaters  
582 of Nalenggele River, where the glacier elevation has reduced by 5.42 m since 2000 (Shen et al.,  
583 2022). However, as a result of the low precipitation in the southwestern basin, achieving  
584 equilibrium in recharge remains a challenge given the rapid melting of ice and snow caused by  
585 climate warming, even if precipitation continues to increase in the future. This means that in the  
586 future climate change scenario, water resources in the southwestern basin watershed (such as  
587 Nalenggele River) may continue to rise for a certain period before showing a large-scale decrease.  
588 This trend of initial increase followed by decrease is common in the Tibetan Plateau or regions  
589 with relatively little precipitation in alpine watersheds around the world. Furthermore, in the  
590 watersheds of the central basin (Nomhon, Golmud, and Yuka Rivers), while the surface–  
591 groundwater recharge is relatively stable, the long-term large-scale exploitation of groundwater in  
592 these three areas during the industrial and agricultural development processes has decreased the  
593 precipitation in the source area and led to a reliance on ice and snow melting. Moreover, a decline  
594 in groundwater level fluctuations in the future is inevitable. Data monitoring of the five shallow  
595 groundwater boreholes in the alluvial fan belt of the Golmud River showed that the groundwater  
596 level has fluctuated and reduced by an average of −1.18 m/a since 2011 (Figure S2). Whether the  
597 increase in water resource renewal capacity and water storage in the Qaidam Basin can remain  
598 stable is a scientific issue that is worthy of consideration in the future.



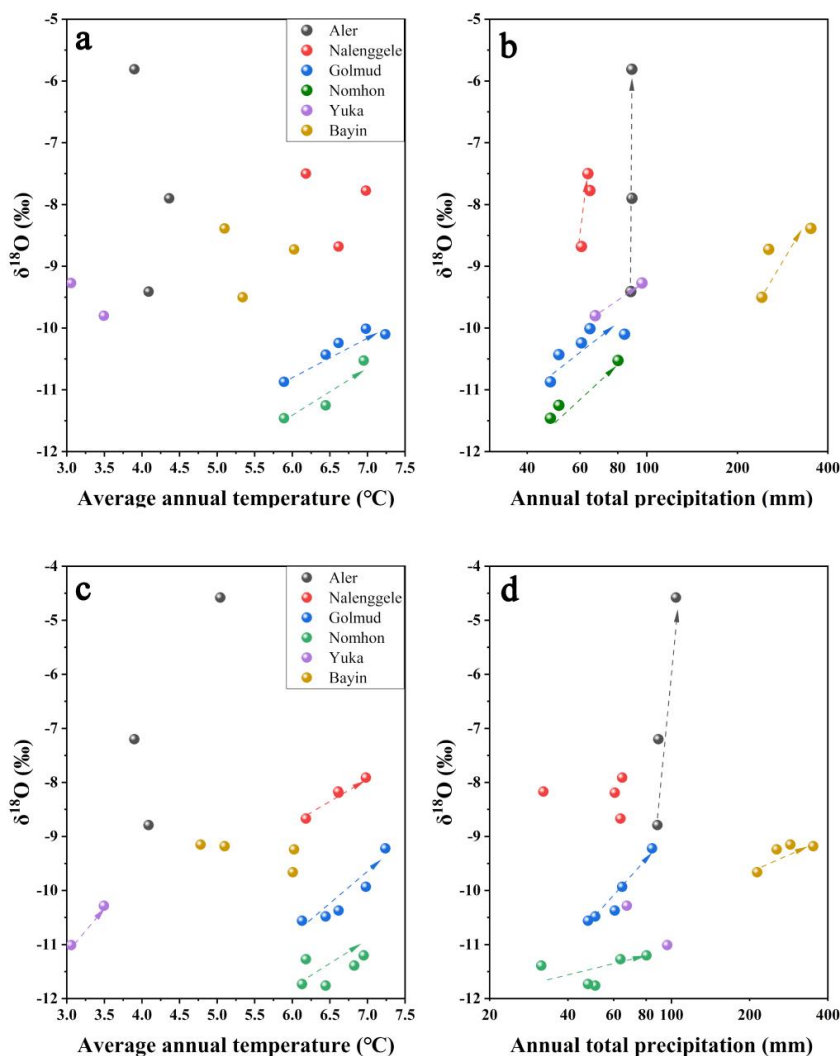
599

600 **Figure 10.** Average temperature and precipitation in the Qaidam Basin every 30 years and 10 years from 1960  
 601 to 2020 (a); interannual changes in temperature and precipitation at the Golmud and Delingha meteorological  
 602 stations (b)



603

604 **Figure 11.** Interannual variations in the river water and groundwater  $\delta^{18}\text{O}$  in the Qaidam Basin



605

606 **Figure 12.** Surface water  $\delta^{18}\text{O}$  and temperature (a) and precipitation (b); Groundwater  $\delta^{18}\text{O}$  and temperature (c)  
607 and precipitation (d) in the Qaidam Basin

## 608 6. Conclusion

609 (1) The contribution of precipitation and ice/snow meltwater is the main factor that drives the  
610 accelerated water cycle in the Qaidam Basin. The spatiotemporal variations of surface water and  
611 groundwater  $\delta^{18}\text{O}$  and  $\delta\text{D}$  reflect their dynamic responses to water sources, climate warming, and  
612 neotectonic movements, especially precipitation, at interannual and seasonal scales. Surface water  
613 H-O isotopes are enriched during the wet season and relatively depleted during the dry season with



614 a remarkable evaporation effect. The mean values of surface water  $\delta^{18}\text{O}$  and  $\delta\text{D}$  in the Eastern  
615 Kunlun Mountains water system are gradually negatively skewed from west to east, and the reverse  
616 holds true for the Qilian Mountains water system. The seasonal differences of isotopes are  
617 determined by the precipitation level and its increase in the watershed, and the spatial change  
618 patterns reflect the influence of water vapor transport intensity of the westerly path and local  
619 climatic conditions. The base flow is maintained by groundwater recharge during the dry season,  
620 and varying proportions of groundwater (26%–62%), ice/snow meltwater (23%–47%) and  
621 precipitation (10%–45%) are received during the wet season. The contribution of precipitation to  
622 surface rivers in the Qilian Mountains is greater than that of the Eastern Kunlun Mountains.

623 (2) The phreatic groundwater system located in the collision and convergent zone of different  
624 mountain ranges is characterized by enriched H-O isotopes, high concentrations of radioactive  $^3\text{H}$ ,  
625 and marked seasonal recharge during the wet season. Modern meltwater and precipitation are able  
626 to infiltrate through favorable structural water channel passages, such as large-scale active fault  
627 zones, giving rise to rapid groundwater recharge. In contrast, the phreatic groundwater systems in  
628 the western region of the Qilian Mountains and the central region of Eastern Kunlun Mountains  
629 have depleted H-O isotopes and low  $^3\text{H}$  concentrations during the wet season, and they are mainly  
630 slowly recharged by seasonal ice/snow meltwater, which consists of modern water and submodern  
631 water (>60 years) maintained together. The confined groundwater is considerably depleted in H-  
632 O isotopes, and a majority has no apparent seasonal changes. The  $^3\text{H}$  concentration is very low or  
633 below the detection limit, and the recharge is relatively slow with fossil water dominated.

634 (3) Climate warming has exerted a substantial impact on the hydrological processes  
635 throughout the whole basin, thereby driving water cycle acceleration and increases in water storage  
636 fluctuations in the eastern and southwestern basin regions via the increase in precipitation and  
637 melting of glaciers and snow. However, the cyclical nature of climate change suggests that this  
638 trend is unsustainable. As precipitation increases and solid water ablation in mountainous regions  
639 becomes severely out of balance, the southwestern basin may face a rapid decline in total water  
640 resources in the future.

641

642



643 **Author Contribution**

644 Conceptualization: Yu Zhang, Hongbing Tan; Funding acquisition: Xiyang Zhang;  
645 Investigation: Peixin Cong; Resources: Wenbo Rao; Visualization: Dongping Shi; Writing–  
646 original draft: Yu Zhang; Writing–review & editing: Hongbing Tan.

647 **Acknowledgments**

648 This study was financially supported by the National Natural Science Foundation of China  
649 (U22A20573) and the Postgraduate Research & Practice Innovation Program of Jiangsu Province  
650 (KYCX22\_0666). We would like to express our gratitude for all members' help both in the field  
651 observation and geochemical analysis in the laboratory.

652 **Declaration of interests**

653 The authors declare that they have no known competing financial interests or personal  
654 relationships that could have appeared to influence the work reported in this paper.

655 **Data Availability Statement**

656 The complete list of isotopes and their values is available in Table S1 in Supporting  
657 Information. The meteorological data can be obtained on China Meteorological Data Network  
658 (<http://data.cma.cn>). The monthly mean ERA5 reanalysis data ( $0.25^\circ \times 0.25^\circ$ ) can be obtained from  
659 European Centre for Medium-Range Weather Forecasts (ECMWF, <https://www.ecmwf.int/>).

660 **References**

- 661 Ahmed, M., Chen, Y., & Khalil, MM (2022). Isotopic Composition of Groundwater Resources  
662 in Arid Environments. *Journal of Hydrology*, 127773.
- 663 Bam, EK, Ireson, AM, van Der Kamp, G., & Hendry, JM (2020). Ephemeral ponds: Are they the  
664 dominant source of depression-focused groundwater recharge?. *Water Resources Research*,  
665 56(3), e2019WR026640.
- 666 Befus, KM, Jasechko, S., Luijendijk, E., Gleeson, T., & Bayani Cardenas, M. (2017). The rapid  
667 yet uneven turnover of Earth's groundwater. *Geophysical Research Letters*, 44(11), 5511-  
668 5520.
- 669 Boutt DF, Mabee SB, Yu Q. Multiyear increase in the stable isotopic composition of stream  
670 water from groundwater recharge due to extreme precipitation[J]. *Geophysical Research*  
671 *Letters*, 2019, 46(10): 5323-5330.



- 672 Bowen, GJ, Cai, Z., Fiorella, RP, & Putman, AL (2019). Isotopes in the water cycle: regional-to  
673 global-scale patterns and applications. *Annual Review of Earth and Planetary Sciences*,  
674 47(1).
- 675 Chang, Q., Ma, R., Sun, Z., Zhou, A., Hu, Y., & Liu, Y. (2018). Using isotopic and geochemical  
676 tracers to determine the contribution of glacier-snow meltwater to streamflow in a partly  
677 glacierized alpine-gorge catchment in northeastern Qinghai-Tibet Plateau. *Journal of*  
678 *Geophysical Research: Atmospheres*, 123(18), 10-037.
- 679 Chatterjee, S., Gusyev, MA, Sinha, UK, Mohokar, HV, & Dash, A. (2019). Understanding water  
680 circulation with tritium tracer in the Tural-Rajwadi geothermal area, India. *Applied*  
681 *Geochemistry*, 109, 104373.
- 682 Chen, C., Zhang, X., Lu, H., Jin, L., Du, Y., & Chen, F. (2021). Increasing summer precipitation  
683 in arid Central Asia linked to the weakening of the East Asian summer monsoon in the  
684 recent decades. *International Journal of Climatology*, 41(2), 1024-1038.
- 685 Chen, J., Wang Y., Zheng, J., & Cao L. (2019). The changes in the water volume of Ayakekumu  
686 Lake based on satellite remote sensing data. *Journal of Natural Resources*, 34(6), 1331-  
687 1344 (in Chinese with English abstract) .
- 688 Condon, LE, Atchley, AL, & Maxwell, RM (2020). Evapotranspiration depletes groundwater  
689 under warming over the contiguous United States. *Nature communications*, 11(1), 1-8.
- 690 Craig, H. (1961). Isotopic variations in meteoric waters. *Science*, 133(3465), 1702-1703.
- 691 Cui, Y., LIU, F., & Hao, Q. (2015). Characteristics of hydrogen and oxygen isotopes and  
692 renewal of groundwater in the Nuomuhong alluvial fan. *Hydrogeology & Engineering*  
693 *Geology*, 42(6), 1-7 (in Chinese with English abstract).
- 694 Dansgaard, W. (1964). Stable isotopes in precipitation. *tellus*, 16(4), 436-468.
- 695 Durack, PJ, Wijffels, SE, & Matear, RJ (2012). Ocean salinities reveal strong global water cycle  
696 intensification during 1950 to 2000. *Science*, 336(6080), 455-458.
- 697 Haddeland, I., Heinke, J., Biemans, H., Eisner, S., Flörke, M., Hanasaki, N., ... & Wisser, D.  
698 (2014). Global water resources affected by human interventions and climate change.  
699 *Proceedings of the National Academy of Sciences*, 111(9), 3251-3256.
- 700 Hooper, RP (2003). Diagnostic tools for mixing models of stream water chemistry. *Water*  
701 *Resources Research*, 39(3), 1055.



- 702 Hooper, RP, Christophersen, N., & Peters, NE (1990). Modeling streamwater chemistry as a  
703 mixture of soilwater end-members—An application to the Panola Mountain catchment,  
704 Georgia, USA. *Journal of Hydrology*, 116(1-4), 321-343.
- 705 Huntington, TG (2006). Evidence for intensification of the global water cycle: review and  
706 synthesis. *Journal of Hydrology*, 319(1-4), 83-95.
- 707 Jasechko, S., Birks, SJ, Gleeson, T., Wada, Y., Fawcett, PJ, Sharp, ZD, ... & Welker, JM (2014).  
708 The pronounced seasonality of global groundwater recharge. *Water Resources Research*,  
709 50(11), 8845-8867.
- 710 Jian, X., Weislogel, A., Pullen, A., & Shang, F. (2020). Formation and evolution of the Eastern  
711 Kunlun Range, northern Tibet: Evidence from detrital zircon U-Pb geochronology and Hf  
712 isotopes. *Gondwana Research*, 83, 63-79.
- 713 Jiao, JJ, Zhang, X., Liu, Y., & Kuang, X. (2015). Increased water storage in the Qaidam Basin,  
714 the North Tibet Plateau from GRACE gravity data. *PloS one*, 10(10), e0141442.
- 715 Juan, G., Li, Z., Qi, F., Ruifeng, Y., Tingting, N., Baijuan, Z., ... & Pengfei, L. (2020).  
716 Environmental effect and spatiotemporal pattern of stable isotopes in precipitation on the  
717 transition zone between the Tibetan Plateau and arid region. *Science of The Total  
718 Environment*, 749, 141559.
- 719 Kang, S., Cong, Z., Wang, X., Zhang, Q., Ji, Z., Zhang, Y., & Xu, B. (2019). The transboundary  
720 transport of air pollutants and their environmental impacts on Tibetan Plateau. *Chinese  
721 Science Bulletin*, 64(27), 2876-2884.
- 722 Ke, L., Song, C., Wang, J., Sheng, Y., Ding, X., Yong, B., ... & Luo, S. (2022). Constraining the  
723 contribution of glacier mass balance to the Tibetan lake growth in the early 21st century.  
724 *Remote Sensing of Environment*, 268, 112779.
- 725 Kong, Y., Wang, K., Pu, T., & Shi, X. (2019). Nonmonsoon precipitation dominates  
726 groundwater recharge beneath a monsoon-affected glacier in Tibetan Plateau. *Journal of  
727 Geophysical Research: Atmospheres*, 124(20), 10913-10930.
- 728 Kuang, X., & Jiao, JJ (2016). Review on climate change on the Tibetan Plateau during the last  
729 half century. *Journal of Geophysical Research: Atmospheres*, 121(8), 3979-4007.
- 730 Li, L., & Garziona, CN (2017). Spatial distribution and controlling factors of stable isotopes in  
731 meteoric waters on the Tibetan Plateau: Implications for paleoelevation reconstruction.  
732 *Earth and Planetary Science Letters*, 460, 302-314.



- 733 Li, L., Shen, H., Li, H., & Xiao, J. (2015). Regional differences of climate change in Qaidam  
734 Basin and its contributing factors. *Journal of Natural Resources*, 30, 641-650 (in Chinese  
735 with English abstract).
- 736 Liu, F., Cui, Y., Zhang, G., Geng, F., & Liu, J. (2014). Using the <sup>3</sup>H and <sup>14</sup>C dating methods to  
737 calculate the groundwater age in Nuomuhong, Qaidam Basin. *Geoscience*, 28 (6), 1322-  
738 1328 (in Chinese with English abstract).
- 739 Liu, J., Song, X., Sun, X., Yuan, G., Liu, X., & Wang, S. (2009). Isotopic composition of  
740 precipitation over Arid Northwestern China and its implications for the water vapor origin .  
741 *Journal of Geographical Sciences*, 19(2), 164-174 (in Chinese with English abstract).
- 742 Malard, A., Sinreich, M., & Jeannin, PY (2016). A novel approach for estimating karst  
743 groundwater recharge in mountainous regions and its application in Switzerland.  
744 *Hydrological Processes*, 30(13), 2153-2166.
- 745 Masson-Delmotte, V., Zhai, P., Pirani, A., Connors, SL, Péan, C., Berger, S., ... & Zhou, B.  
746 (2021). Climate change 2021: the physical science basis. Contribution of working group I to  
747 the sixth assessment report of the intergovernmental panel on climate change, 2.
- 748 Moran, BJ, Boutt, DF, & Munk, LA (2019). Stable and radioisotope systematics reveal fossil  
749 water as fundamental characteristic of arid orogenic-scale groundwater systems. *Water*  
750 *Resources Research*, 55(12), 11295-11315.
- 751 Parnell, AC, Inger, R., Bearhop, S., & Jackson, AL (2010). Source partitioning using stable  
752 isotopes: coping with too much variation. *PloS one*, 5(3), e9672.
- 753 Shen, C., Jia, L., & Ren, S. (2022). Inter-and Intra-Annual Glacier Elevation Change in High  
754 Mountain Asia Region Based on ICESat-1&2 Data Using Elevation-Aspect Bin Analysis  
755 Method. *Remote Sensing*, 14(7), 1630.
- 756 Shi, D., Tan, H., Chen, X., Rao, W., & Basang, R. (2021). Uncovering the mechanisms of  
757 seasonal river-groundwater circulation using isotopes and water chemistry in the middle  
758 reaches of the Yarlungzangbo River, Tibet. *Journal of Hydrology*, 603, 127010.
- 759 Song, C., Huang, B., Richards, K., Ke, L., & Hien Phan, V. (2014). Accelerated lake expansion  
760 on the Tibetan Plateau in the 2000s: Induced by glacial melting or other processes?. *Water*  
761 *Resources Research*, 50(4), 3170-3186.



- 762 Tan, H., Zhang, Y., Rao, W., Guo, H., Ta, W., Lu, S., & Cong, P. (2021). Rapid groundwater  
763 circulation inferred from temporal water dynamics and isotopes in an arid system.  
764 *Hydrological Processes*, 35(6), e14225.
- 765 Tian, L., Yao, T., Sun, W., Stievenard, M., & Jouzel, J. (2001). Relationship between  $\delta D$  and  
766  $\delta^{18}O$  in precipitation on north and south of the Tibetan Plateau and moisture recycling.  
767 *Science in China Series D: Earth Sciences*, 44(9), 789-796.
- 768 Wang, L., Yao, T., Chai, C., Cuo, L., Su, F., Zhang, F., Yao, Z., Zhang, Y., Li, X., Qi, J., Hu, Z.,  
769 Liu, J., & Wang, Y. (2021). TP-River: Monitoring and Quantifying Total River Runoff  
770 from the Third Pole, *Bulletin of the American Meteorological Society*, 102(5), E948-E965.
- 771 Wang, S., Lei, S., Zhang, M., Hughes, C., Crawford, J., Liu, Z., & Qu, D. (2022). Spatial and  
772 seasonal isotope variability in precipitation across China: Monthly isoscapes based on  
773 regionalized fuzzy clustering. *Journal of Climate*, 35(11), 3411-3425.
- 774 Wang, X., Chen, M., Gong, P., & Wang, C. (2019). Perfluorinated alkyl substances in snow as  
775 an atmospheric tracer for tracking the interactions between westerly winds and the Indian  
776 Monsoon over western China. *Environment international*, 124, 294-301.
- 777 Wang, X., Yang, M., Liang, X., Pang, G., Wan, G., Chen, X., & Luo, X. (2014). The dramatic  
778 climate warming in the Qaidam Basin, northeastern Tibet Plateau, during 1961–2010.  
779 *International Journal of Climatology*, 34(5), 1524-1537.
- 780 Wang, Y., Guo, H., Li, J., Huang, Y., Liu, Z., Liu, C., Guo, X., Zhou, J., Shang, X., Li, J.,  
781 Zhuang, Y., & Cheng, H. (2008). Investigation and assessment of groundwater resources  
782 and their environmental issues in the Qaidam Basin. Geological Publishing House.
- 783 Wei, L., Jiang, S., Ren, L., Tan, H., Ta, W., Liu, Y., ... & Duan, Z. (2021). Spatiotemporal  
784 changes of terrestrial water storage and possible causes in the closed Qaidam Basin, China  
785 using GRACE and GRACE Follow-On data. *Journal of Hydrology*, 598, 126274.
- 786 Wu, H., Zhang, C., Li, XY, Fu, C., Wu, H., Wang, P., & Liu, J. (2022). Hydrometeorological  
787 Processes and Moisture Sources in the Northeastern Tibetan Plateau: Insights from a 7-Yr  
788 Study on Precipitation Isotopes. *Journal of Climate*, 35(20), 2919-2931.
- 789 Xiang, L., Wang, H., Steffen, H., Wu, P., Jia, L., Jiang, L., & Shen, Q. (2016). Groundwater  
790 storage changes in the Tibetan Plateau and adjacent areas revealed from GRACE satellite  
791 gravity data. *Earth and Planetary Science Letters*, 449, 228-239.



- 792 Xiao, Y., Shao, J., Cui, Y., Zhang, G., & Zhang, Q. (2017). Groundwater circulation and  
793 hydrogeochemical evolution in Nomhon of Qaidam Basin, northwest China. *Journal of*  
794 *Earth System Science*, 126 (2), 1-16.
- 795 Xiao, Y., Shao, J., Frapce, SK, Cui, Y., Dang, X., Wang, S., & Ji, Y. (2018). Groundwater origin,  
796 flow regime and geochemical evolution in arid endorheic watersheds : a case study from the  
797 Qaidam Basin, northwestern China. *Hydrology and Earth System Sciences*, 22(8), 4381-  
798 4400.
- 799 Xu, W., Su, X., Dai, Z., Yang, F., Zhu, P., & Huang, Y. (2017). Multi-tracer investigation of  
800 river and groundwater interactions: a case study in Nalenggele River basin, northwest  
801 China. *Hydrogeology Journal*, 25(7), 2015-2029.
- 802 Yang, N., & Wang, G. (2020). Moisture sources and climate evolution during the last 30 kyr in  
803 northeastern Tibetan Plateau: Insights from groundwater isotopes (2H, 18O, 3H and 14C)  
804 and water vapor trajectories modeling. *Quaternary Science Reviews*, 242, 106426.
- 805 Yang, N., Wang, G., Liao, F., Dang, X., & Gu, X. (2023). Insights into moisture sources and  
806 evolution from groundwater isotopes (2H, 18O, and 14C) in Northeastern Qaidam Basin,  
807 Northeast Tibetan Plateau, China. *Science of The Total Environment*, 864, 160981.
- 808 Yang, N., Zhou, P., Wang, G., Zhang, B., Shi, Z., Liao, F., ... & Gu, X. (2021). Hydrochemical  
809 and isotopic interpretation of interactions between surfaces water and groundwater in  
810 Delingha, Northwest China. *Journal of Hydrology*, 598, 126243.
- 811 Yang, Y., Wu, Q., & Jin, H. (2016). Evolutions of water stable isotopes and the contributions of  
812 cryosphere to the alpine river on the Tibetan Plateau. *Environmental Earth Sciences*, 75(1),  
813 1-11 .
- 814 Yao, T., Bolch, T., Chen, D., Gao, J., Immerzeel, W., Piao, S., ... & Zhao, P. (2022). The  
815 imbalance of the Asian water tower. *Nature Reviews Earth & Environment*, 1-15.
- 816 Yao, T., Masson-Delmotte, V., Gao, J., Yu, W., Yang, X., Risi, C., ... & Hou, S. (2013). A  
817 review of climatic controls on  $\delta^{18}\text{O}$  in precipitation over the Tibetan Plateau: Observations  
818 and simulations. *Reviews of Geophysics*, 51(4), 525-548.
- 819 Zhang, G., Yao, T., Shum, CK, Yi, S., Yang, K., Xie, H., ... & Yu, J. (2017). Lake volume and  
820 groundwater storage variations in Tibetan Plateau's endorheic basin. *Geophysical Research*  
821 *Letters*, 44(11), 5550-5560.



- 822 Zhang, Q., Zhu, B., Yang, J., Ma, P., Liu, X., Lu, G., ... & Wang, D. (2021). New characteristics  
823 about the climate humidity trend in Northwest China. *Chinese Science Bulletin*, 66, 3757-  
824 3771.
- 825 Zhang, X., Chen, J., Chen, J., Ma, F., & Wang, T. (2022). Lake Expansion under the  
826 Groundwater Contribution in Qaidam Basin, China. *Remote Sensing*, 14(7), 1756 .
- 827 Zhao, D., Wang, G., Liao, F., Yang, N., Jiang, W., Guo, L., ... & Shi, Z. (2018). Groundwater-  
828 surface water interactions derived by hydrochemical and isotopic ( $^{222}\text{Rn}$ , deuterium,  
829 oxygen-18) tracers in the Nomhon area, Qaidam Basin, NW China. *Journal of Hydrology*,  
830 565, 650-661.
- 831 Zhao, D., Wang, G., Liao, F., Yang, N., Jiang, W., Guo, L., ... & Shi, Z. (2018). Groundwater-  
832 surface water interactions derived by hydrochemical and isotopic ( $^{222}\text{Rn}$ , deuterium,  
833 oxygen-18) tracers in the Nomhon area, Qaidam Basin, NW China. *Journal of Hydrology*,  
834 565, 650-661.
- 835 Zhao, L., Yin, L., Xiao, H., Cheng, G., Zhou, M., Yang, Y., ... & Zhou, J. (2011). of surface  
836 runoff in the headwaters of the Heihe River basin. *Chinese Science Bulletin*, 56(4), 406-  
837 415.
- 838 Zhu, J., Chen, H., & Gong, G. (2015). Hydrogen and oxygen isotopic compositions of  
839 precipitation and its water vapor sources in Eastern Qaidam Basin. *Environmental Science*,  
840 36(8), 2784-2790 (in Chinese with English abstract).
- 841 Zou, Y., Kuang, X., Feng, Y., Jiao, JJ, Liu, J., Wang, C., ... & Zheng, C. (2022). Solid water melt  
842 dominates the increase of total groundwater storage in the Tibetan Plateau. *Geophysical*  
843 *Research Letters*, e2022GL100092.
- 844